Quasinormal Modes and Phase Structure of Regular AdS Einstein-Gauss-Bonnet Black Holes

Yerlan Myrzakulov,[1,2,*] Kairat Myrzakulov,[1,†] Sudhaker Upadhyay[cd,3,4,¶] and Dharm Veer Singh[f5,††]

[1]*Department of General & Theoretical Physics, L. N. Gumilyov Eurasian National University, Astana, 010008, Kazakhstan*
[2]*Ratbay Myrzakulov Eurasian International Centre for Theoretical Physics Astana 010009, Kazakhstan*
[3]*Department of Physics, K. L. S. College, Magadh University,*
Nawada 805110, India
[4]*School of Physics, Damghan University, P.O. Box 3671641167,*
Damghan, Iran
[5]*Department of Physics, Institute of Applied Sciences and Humanities,*
GLA University, Mathura 281406, Uttar Pradesh, India.

In this paper, we present an exact regular black hole solution in Einstein-Gauss-Bonnet coupled with nonlinear matter fields. It is a generalization of a regular Einstein-Gauss-Bonnet black hole in $5D$ AdS spacetime. The causal structure of the obtained solution identifies with Boulware-Deser black hole solution, except for the curvature singularity at the center. It incorporates the Boulware-Deser black holes in the absence of deviation parameters. We also study the thermodynamic properties of the solution that satisfies a modified first law of thermodynamics. Furthermore, we discuss the stability of the obtained black hole solution and, in this regard, a double phase transition occurs. Within context, we find that phase transition exists at the point where the heat capacity diverges and, incidentally, the temperature attains the maximum value. We discuss the fluid nature of the black hole also exhibiting critical points. The quasinormal modes of the black hole solution and their dependencies on Gauss-Bonnet coupling and deviation parameters are also analysed in terms of null geodesics.

Keywords: Quasinormal modes; $5D$ EGB Black hole; Phase transition.

I. INTRODUCTION

The higher-order curvature theories are useful to explore various (conceptual) concerns of gravity. Lovelock's theory of gravity [1–3] is one of such higher-order curvature gravity that generalizes the general relativity (GR) to higher spacetime dimensions. In Ref. [1], Lovelock proposed that GR in $4D$ with a cosmological constant possessing diffeomorphism invariance, metricity and second-order equations of motion is a unique theory of pure gravity. The Einstein-Gauss-Bonnet (EGB) gravity is a particular class of Lovelock gravity that characterizes non-trivial dynamics for the higher-dimensional gravity having second-order field equations. However, EGB gravity in $4D$ is a topological theory that, in general, does not contribute to gravitational dynamics. In the recent past, a lot of efforts have been made to study the EGB gravity in $4D$. For instance, Glavan and Lin proposed the $4D$ GB theory by re-scaling the GB coupling constant. But the theory in $D = 4$ limit is either plagued by the partial breaking of diffeomorphism or by additional gravitational degrees of freedom. The generalization of EGB gravity as F(GB) gravity in $4D$ was presented in Refs [4, 5]. In another effort, EGB gravity in $4D$ is constructed that has only two dynamical degrees of freedom but it breaks the temporal diffeomorphism [6, 7].

Black holes are one of the most fascinating objects and the subjects of active research. Black holes are either singular or regular solutions of the Einstein equation of GR. A singular solution for the rotating counterpart of a higher-derivative theory in Lee-Wick prescription is explored recently [8]. The first spherically symmetric regular black hole solution was given by Bardeen [9] that does not hold a strong energy condition. In the recent past, people are paying much attention to the regular black hole solutions [10–17]. An exact regular black hole solution for the EGB coupled with non-Abelian gauge field in 4D AdS spacetime and their thermal properties are explored recently [18]. Recently, a $4D$ AdS EGB black hole solution with nonlinear electrodynamics (NLED) is studied [19]. In another recent work, the EGB massive black hole solution in $4D$ AdS is studied also [20–23].

The NLED in the context of black hole physics is a more relevant and quite suitable alternative for Maxwell (linear) electrodynamics as we know that the real electromagnetic field remains no longer linear at high energy due to the

[c] Corresponding author
[d] Visiting Associate, IUCAA Pune, Maharashtra 411007, India
[f] Visiting Associate, IUCAA Pune, Maharashtra 411007, India
[*] ymyrzakulov@gmail.com
[†] krmyrzakulov@gmail.com
[¶] sudhakerupadhyay@gmail.com
[††] veerdsingh@gmail.com

influence of other physical fields. Since the original consideration of nonlinear electrodynamics by Born and Infeld [24], extensive progresses on the subject has been made [25–29]. Some NLED coupled to GR may provide a better explanation for the inflation of the universe [30–33]. Black holes with NLED are quite relevant in astrophysical observations [34, 35].

The advantage of the study of NLED field coupled with the gravity, we obtained the regular black hole solution in the particular limits it correctly retrieves the Reissner-Nordstrom black hole. Another major difference is in the strong-field limits of Einstein's gravity, where the exponential mass function leads to a Minkowski-flat core around, which is in striking contrary with other regular black holes [36, 37] that generally have de-Sitter core [38–40]. Therefore, the curvature of the geometry has some maximal peak in between spatial infinity and core. Although, in the $4D$ EGB gravity, all regular black holes have flat core around them [4, 5]. Therefore, this novel regular black hole share many features with other regular black holes, but there are also significant differences.

The AdS/CFT correspondence [41–43] provides a duality between strong interacting quantum field theory and weakly interacting gravity. This is also known as the holographic duality or the gauge/gravity duality. GB term in such correspondence may play an important role, see Refs. [44, 45]. Originally, this was explored in the context of string theory but further extended to wide domains, such as the coupling dynamics of QCD and the electroweak theories, black holes physics, quantum gravity, condensed matter physics, etc. In the context of black holes, Witten found that black hole thermodynamics in AdS spaces can get a resemblance with the thermodynamics of dual CFT at the high temperature [46].

The concept of black hole thermodynamics originated by Bekenstein [47, 48] and Hawking [49] who realized that entropy is somehow connected to the area of the Black hole horizon. To a certain extent, it is clear that entropy of the black holes is proportional to the area of horizon [50–53]. This subject was studied further extensively [54–59] In the context of black hole thermodynamics (mechanics), it is found that the black hole system satisfies the first law of thermodynamics. The stability of dS and Nariai black hole in higher derivative gravity is discussed in Ref. [60]. Here, it is found that for certain regime Nariai black hole is stable and does not decay into pure de Sitter space. The this connection of higher derivative gravity, negative (or zero) Schwarzschild-(Anti)-de Sitter black entropy is found which depends on the parameters of higher derivative terms [21].

Quasinormal modes (QNMs) have been found an active and wide area of research [61–64]. QNMs are found very useful to predict the stability of the perturbed black holes. Abbott et al. (LIGO scientific collaboration and Virgo collaboration) detected transient gravitational waves [65]. The images of Event Horizon Telescope [66] display a prominent ring consistent with the size and shape of the lensed photon shadow of a supermassive black hole. These studies hint about the correspondence between QNMs and black hole shadow radius. The correspondence between QNMs and shadow radius may provide a new viewpoint for the gravitational waves which are massless particles moving along an outmost unstable orbit of null geodesics. Recently, the shadow cast of the charged Reissner-Nordström AdS black hole in both plasma and non-plasma medium is studied [67].

The rest of the sections are organized as follows. In Sec. II, we consider a EGB gravity coupled to the NLED in $5D$ AdS spacetime and obtain a new black hole solution. We discuss the horizon structure of this new black hole solution in AdS spacetime. The thermodynamics of this black hole along with stability and phase transition are discussed in section III. The behavior of black holes as the Van der Waals fluid is reported in section IV. We have calculated the critical values of pressure, temperature, and horizon radius and their dependencies on various parameters. The QNMs for the black hole solution are calculated in section V. Finally, we summarize the results and make final remarks in the last section.

II. ACTION, BLACK HOLE SOLUTIONS AND HORIZON STRUCTURE

For the present study, we are interested in the solution of $5D$ EGB gravity coupled to the NLED in AdS space. The action describing $5D$ EGB gravity coupled to the NLED in AdS spacetime is written as [68]

$$S = \frac{1}{2} \int d^5x \sqrt{-g} \left[R - 2\Lambda + \alpha(R_{\mu\nu\gamma\delta}R^{\mu\nu\gamma\delta} - 4R_{\mu\nu}R^{\mu\nu} + R^2) - 4P\frac{\partial\mathcal{H}}{\partial P} + 2\mathcal{H} \right], \tag{1}$$

where R, $R_{\mu\nu}$ and $R_{\mu\nu\lambda\sigma}$ are the Ricci scalar, Ricci tensor and Riemann tensor, respectively. However, Λ and α are the cosmological constant related to AdS length l via relation $-3/l^2$ and the Gauss-Bonnet coupling constant, respectively. $\mathcal{H}(P)$ is the structure- function that depends on the invariant $P = \frac{1}{4}P_{\mu\nu}P^{\mu\nu}$ of the tensor $P_{\mu\nu}$ which corresponds to electric induction. The expression for the NLED structure function $\mathcal{H}(P)$ is given by

$$\mathcal{H}(P) = 3Pe^{-\frac{q}{M}(-2qP)^{1/3}}, \tag{2}$$

where q and M are the free parameters associated with the charge and mass, respectively. In the weak field limit $(P << 1)$, the NLED structure function (2) corresponds to the linear electrodynamics, i.e. $\mathcal{H}(P) \approx P$. The requirements to satisfy the weak energy condition are $\mathcal{H} < 0$ and $\frac{\partial \mathcal{H}}{\partial P} > 0$ [69–71].

The field equations corresponding to the action (1) for the metric tensor $(g_{\mu\nu})$ and electromagnetic potential (A_μ) are

$$G_{\mu\nu} + H_{\mu\nu} + \Lambda g_{\mu\nu} = 2 \left(\frac{\partial \mathcal{H}}{\partial P} P_{\mu\lambda} P_\nu^\lambda - 2P \frac{\partial \mathcal{H}}{\partial P} + \mathcal{H} \right), \tag{3}$$

$$\nabla_\mu P^{\mu\nu} = 0, \tag{4}$$

where G_{ab} and H_{ab} are, respectively

$$G_{\mu\nu} = R_{\mu\nu} - \frac{1}{2} g_{\mu\nu} R, \tag{5}$$

$$H_{\mu\nu} = -\frac{\alpha}{2} \left[8R^{\rho\sigma} R_{\mu\rho\nu\sigma} - 4R_\mu^{\rho\sigma\lambda} R_{\nu\rho\sigma\lambda} - 4RR_{\mu\nu} + 8R_{\mu\lambda} R_\nu^\lambda \right.$$
$$\left. + g_{\mu\nu} \left(R_{\mu\nu\gamma\delta} R^{\mu\nu\gamma\delta} - 4R_{\mu\nu} R^{\mu\nu} + R^2 \right) \right], \tag{6}$$

Now, we are interested to obtain a $5D$ EGB black hole solution in the presence of NED. For this, we first write the static spherically symmetric metric as follows:

$$ds^2 = -f(r)dt^2 + \frac{1}{f(r)} dr^2 + r^2(d\theta^2 + \sin^2\theta d\phi^2 + \sin^2\theta \sin^2\phi \, d\psi^2), \tag{7}$$

where $f(r)$ is the metric function which will be determined later.

We use the following ansatz for the antisymmetric field:

$$P_{\mu\nu} = 2\delta_{[\mu}^\theta \delta_{\nu]}^\phi D(r) \sin^2\theta \sin\phi, \tag{8}$$

which, upon integration (4), eventually leads to

$$P = \frac{q^2}{2r^6}. \tag{9}$$

Here, we chose the integration constant as q.

With this antisymmetric field $P_{\mu\nu}$ and invariant P, the non-vanishing component of Einstein field equation (3) results

$$(4\alpha f' - 2r)(f - 1) - r^3 f' - \Lambda r^2 = \frac{2Mk}{r^3} e^{-k/r^2}, \tag{10}$$

where the prime ($'$) is the derivative of the metric function $f(r)$ concerning r and deviation parameter $k = q^2/M$. The solution of Eq. (10) determines the form of metric function as

$$f(r) = 1 + \frac{r^2}{4\alpha} \left(1 \pm \sqrt{1 + \frac{8M\alpha}{r^4} e^{-k/r^2} + \frac{8\Lambda\alpha}{3}} \right). \tag{11}$$

We note that the solution (12) has two branches, $+ve$ and $-ve$, respectively.

For vanishing Mass, the obtained black hole solution (12) becomes

$$f(r) = 1 + \frac{r^2}{4\alpha} \left(1 \pm \sqrt{1 - \frac{8\alpha}{l^2}} \right). \tag{12}$$

For $\alpha > 0$, $8\alpha/l^2 \leq 1$ and beyond this, there is no black hole solution. Thus, the action 1 has two AdS solutions with effective cosmological constants $l_{eff}^2 = \frac{l^2}{4} \left(1 \pm \sqrt{1 - \frac{8\alpha}{l^2}} \right)$. For $8\alpha/l^2 = 1$, both the solutions coincide and, therefore, the theory has a unique AdS vacuum.

When $\alpha < 0$, the solution (12) still remains AdS for $-ve$ signature and becomes dS if one takes the $+ve$ signature. From the vacuum case, the solution (12) with both signs seems reasonable, from which we cannot determine which sign should be adopted. Then Boulware and Deser showed that the solution with $+ve$ branch is unstable and the solution is asymptotically an AdS Schwarzschild solution with negative gravitational mass, indicating the instability.

The solution (12) with $-ve$ branch is stable and the solution is asymptotically a Schwarzschild solution. Therefore the $+ve$ branch is of less physical interest [44, 45]

This describes a $5D$ AdS regular black hole for EGB gravity coupled with NLED. The resulting black hole is characterized by parameters like M, k and α. In the limit, $\alpha \to 0$ and $k = 0$, the negative branch of solution (11) corresponds to the $5D$ Schwarzschild-Tangherlini black hole. However, in the limit $\alpha \to 0$, the solution (11) corresponds to the regular Schwarzschild black hole in $5D$ AdS [71, 72]

$$f(r) = \left(1 - \frac{2Me^{-k/r^2}}{r^2} - \frac{\Lambda r^2}{3}\right). \tag{13}$$

Here, we remark that the exponential factor present in the solution removes the curvature singularity. The given metric (11) can also be considered as the EGB black hole coupled to NLED. It can be checked that solution (11) matches with the Boulware-Deser black hole provided the mass (M) must be replaced with $M(r)$:

$$M(r) = \frac{\sigma(r)}{\sigma_\infty}M, \tag{14}$$

where $\sigma(r) = e^{-k/r^2}$ is the probability distribution function satisfying $\sigma(r) \geq 0$ and $\sigma'(r) < 0$ for $r \geq 0$. Also, $\sigma(r)/r \to 0$ for $r \to 0$ and σ_∞ refers to is the probability distribution function when $r \to \infty$. Asymptotically $((r >> k))$, the metric (11) corresponds to the charged AdS EGB black hole [73]

$$f(r) = 1 + \frac{r^2}{4\alpha}\left(1 \pm \sqrt{1 + \frac{8\alpha M}{r^4} - \frac{8\alpha q^2}{r^6} + \frac{8\Lambda\alpha}{3}}\right). \tag{15}$$

Henceforth, we end up with a new solution describing an exact regular EGB black hole coupled with nonlinear matter fields in AdS space. This AdS solution, characterized by the parameter M and k, extends the Wiltshire charged EGB black hole [73] to AdS space.

The horizon of the black hole is described by the following condition:

$$1 + \frac{r^2}{4\alpha}\left(1 \pm \sqrt{1 + \frac{8M\alpha}{r^4}e^{-\frac{k}{r^2}} + \frac{8\Lambda\alpha}{3}}\right) = 0. \tag{16}$$

The plot for $f(r)$ versus r is depicted in FIG. 1. Eq. (16) is a complex expression that complicates the analysis of
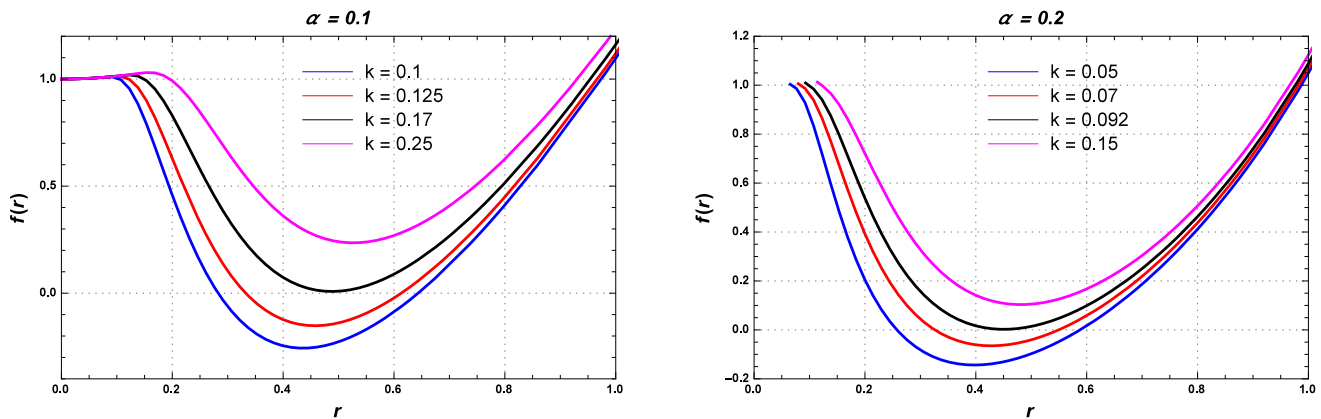

FIG. 1. The metric function $f(r)$ versus r with different value of deviation parameter k for $\alpha = 0.1$ (left panel) and $\alpha = 0.2$ (right panel) with fixed M and l.

the horizon structure analytically. Henceforth, we prefer numerical analysis of the horizon condition by varying the deviation parameter k. The horizon condition $f(r) = 0$ will find two real roots, namely, r_+ and r_- that correspond to the event and Cauchy horizon, respectively. The numerical values of r_- and r_+ for different α and k are tabulated in Table I. The horizons can also be discussed in terms of the deviation parameter k. Now, it is possible to compute the value of k which satisfies the horizon condition that admits two real roots for r. From the table, it is evident that there exists a critical horizon $r_c = r_\pm = 0.483$ and critical deviation parameter $k_c = 0.17$ for $\alpha = 0.1$. However, a critical horizon $r_c = r_\pm = 0.447$ and critical deviation parameter $k_c = 0.092$ exist for $\alpha = 0.2$. These signify extremal regular AdS black holes. Moreover, $k < k_c$ for $\alpha = 0.1$ and $k > k_c$ for $\alpha = 0.2$, the two different horizons $(r_\pm)$ signify the non-extremal black hole. We find that the size of the black hole decreases with an increase in the value of α.

$\alpha = 0.1$				$\alpha = 0.2$			
k	r_-	r_+	δ	k	r_-	r_+	δ
0.1	0.283	0.643	0.360	0.1	0.258	0.596	0.338
0.125	0.329	0.612	0.283	0.07	0.329	0.558	0.229
0.17	0.483	0.483	0	0.092	0.447	0.447	0

TABLE I. Cauchy horizon (r_-). event horizon (r_+), and $\delta = r_+ - r_-$ for the $5D$ AdS EGB Bardeen black hole with $\alpha = 0.1$ and $\alpha = 0.2$ with fixed M and Λ.

III. THERMODYNAMICS

Now, we can study the thermodynamic properties of the obtained black hole solution in terms of horizon radius, which are described by the horizon mass (M_+), deviation parameter (k), and the cosmological constant Λ. The horizon mass and Hawking temperature (T_+) is calculated by

$$M_+ = e^{k/r_+^2} \left(\frac{r_+^4}{l^2} + (r_+^2 + 2\alpha) \right), \tag{17}$$

$$T_+ = \frac{1}{4\pi} \frac{\partial}{\partial r} \sqrt{-g^{rr}g_{tt}} \Big|_{r=r_+} = \frac{r_+^4 - k(r_+^2 + 2\alpha)}{2\pi r_+^3 (r^2 + 4\alpha)} + \frac{2r_+^6 - kr_+^4}{2l^2 \pi r_+^3 (r_+^2 + 4\alpha)}. \tag{18}$$

The Hawking temperature is characterized by k, α, and Λ. The temperature of this regular AdS black hole is plotted in FIG. 2. From the figure, we see that the effect of the deviation parameter is more significant for small black holes.
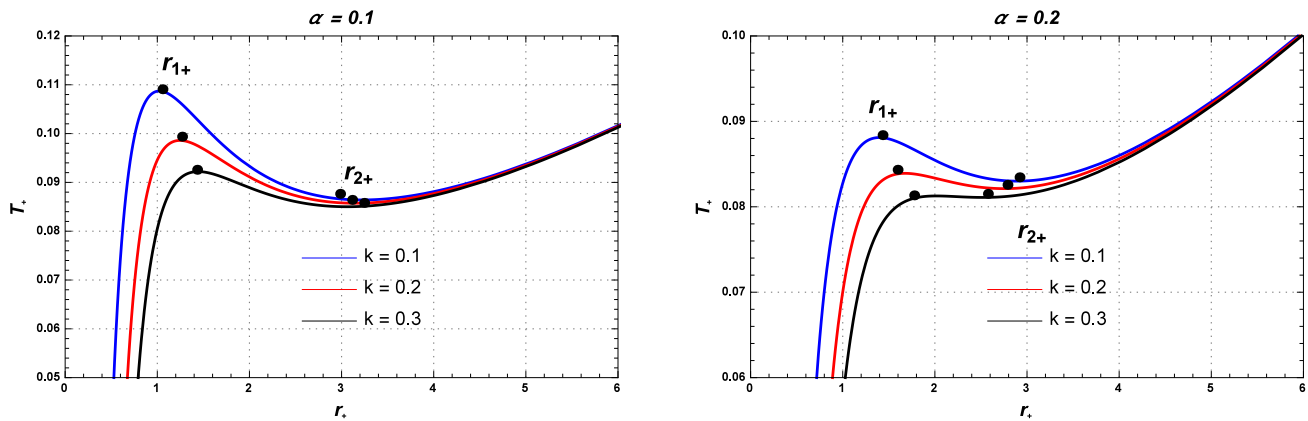

FIG. 2. Temperature T_+ versus r_+ for distinct value of deviation parameter k with $\alpha = 0.1$ (left panel) and $\alpha = 0.2$ (right panel) with fixed $M = 1$ and $l = 10$.

As the value of k increases, the peak of the temperature decreases and occurs at larger r_+ as well. The temperature of the AdS regular black hole also decreases with an increase in α and shifts toward the large value of the horizon radius.

Being a thermal system, the black hole follows the first law of thermodynamics given by

$$dM_+ = T_+ dS_+ + \phi de, \tag{19}$$

where S_+ refers to the entropy of the black hole. For the given values of M_+ and T_+, the first law of thermodynamics leads to the following expression for the entropy:

$$S_+ = \frac{4\pi r_+^3}{3} \left[\frac{(2k + r_+^2 + 12\alpha)e^{k/r_+^2}}{r_+^2} - \frac{2\sqrt{\pi k}\,(4k + 6\alpha)}{r_+^3} \mathrm{erf}\left(\frac{\sqrt{k}}{r_+} \right) \right], \tag{20}$$

where erf is the error function. Here, we note that the entropy matches with the one calculated in Ref. [36] without the cosmological constant. The deformed entropy from the area-law occurs due to the presence of deviation parameters and GB parameter.

We know that entropy of the regular black hole does not follow the area law [74, 75] because the black hole mass is included in the source term. Ma *et al* [76] proposed the corrected form of first law black hole thermodynamics for regular black holes which modifies with the extra factor. The modified first law is [37, 76, 77]

$$C_M dM = T_+ dS + \phi \, de, \tag{21}$$

where $C(M, r_+)$ is

$$C(M, r_+) = 1 + 4\pi \int_{r_+}^{\infty} r^2 \frac{\partial T_0^0}{\partial M} dr = 2e^{-k/r_+^2}. \tag{22}$$

For this value of $C(M, r_+)$ and the obtained black hole solution follows the area law.

The thermodynamic stability of the given black hole can be explained by the nature of the heat capacity as the positive and negative signatures of heat capacity justify the stable and unstable state of the black hole, respectively. The heat capacity for the black hole solution can be defined as

$$C_+ = \frac{\partial M_+}{\partial T_+}. \tag{23}$$

For the given mass (17) and temperature (18), the expression of the heat capacity reads

$$C_+ = \frac{4e^{\frac{k}{r_+^2}} \pi r (r_+^2 + 4\alpha)^2 (r_+^4 (l^2 + 2r_+^2) - k(r_+^4 + l^2(r_+^2 + 2\alpha)))}{2r_+^6 (r_+^2 + 12\alpha) - l^2(r_+^6 - 4r_+^4 \alpha) + k(r_+^6 - 4r_+^4 \alpha + l^2(3r_+^4 + 14r_+^2 \alpha + 24\alpha^2))}. \tag{24}$$

From this expression, it is cumbersome to identify the signature and behavior of heat capacity. Hence, we plot the heat capacity as depicted in diagram 3 for different values of deviation parameter k. To study the nature of the
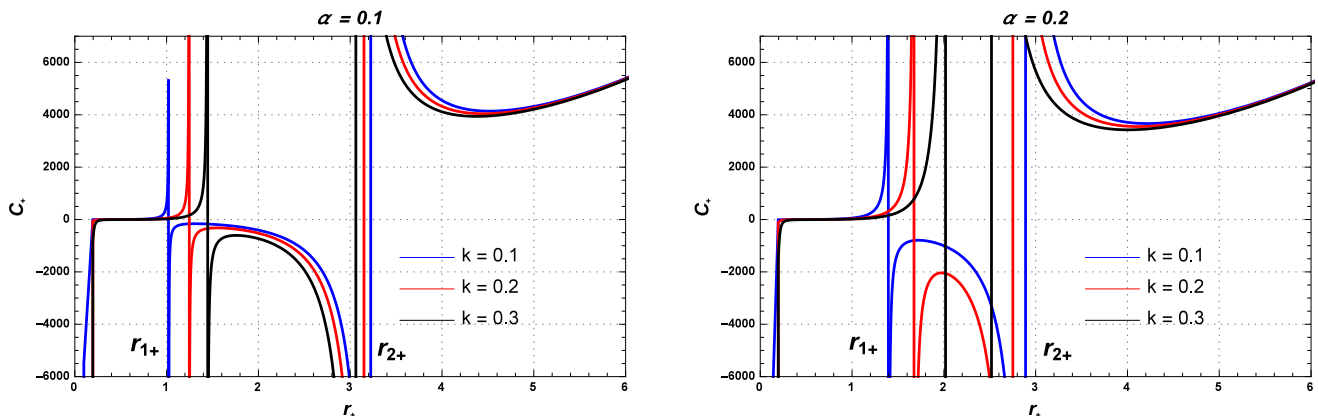

FIG. 3. The heat capacity C_+ versus r_+ with different value of deviation parameter k for $\alpha = 0.1$ (left panel) and $\alpha = 0.2$ (right panel) with fixed value of $M = 1$ and $l = 10$.

heat capacity, we plotted them for the various values of k and α. From the FIG. 3, we find that there exist double phase transitions. Firstly, a phase transition occurs from a small stable black hole to a large unstable black hole and, secondly, from a smaller unstable black hole to a larger stable black hole. For the fixed value of α the radii r_{1+} increases and r_{2+} decreases with k.

Gibbs free energy also plays an important role in order to discuss the (global) stability of the black hole. The Gibbs free energy can be calculated from the standard definition: $G_+ = M_+ - T_+ S_+$. This yields

$$G_+ = e^{k/r_+^2} \left(\frac{r_+^4}{l^2} + (r_+^2 + 2\alpha) \right) - \frac{2}{3} \left(\frac{r_+^4 (l^2 + 2r_+^2) - k(r_+^4 + l^2(r_+^2 + 2\alpha))}{l^2(r_+^2 + 4\alpha)} \right)$$
$$\times \left[\frac{(2k + r_+^2 + 12\alpha)e^{k/r_+^2}}{r_+^2} - \frac{2\sqrt{\pi k}\,(4k + 6\alpha)}{r_+^3} \mathrm{erf}\left(\frac{\sqrt{k}}{r_+} \right) \right]. \tag{25}$$

The stability can also be explained from the Gibbs free energy plot as depicted in FIG. 4. From the plot, we observe that the free energy exhibits local minima (r_{1+}) and local maxima (r_{2+}) for distinct values of k with fixed value of
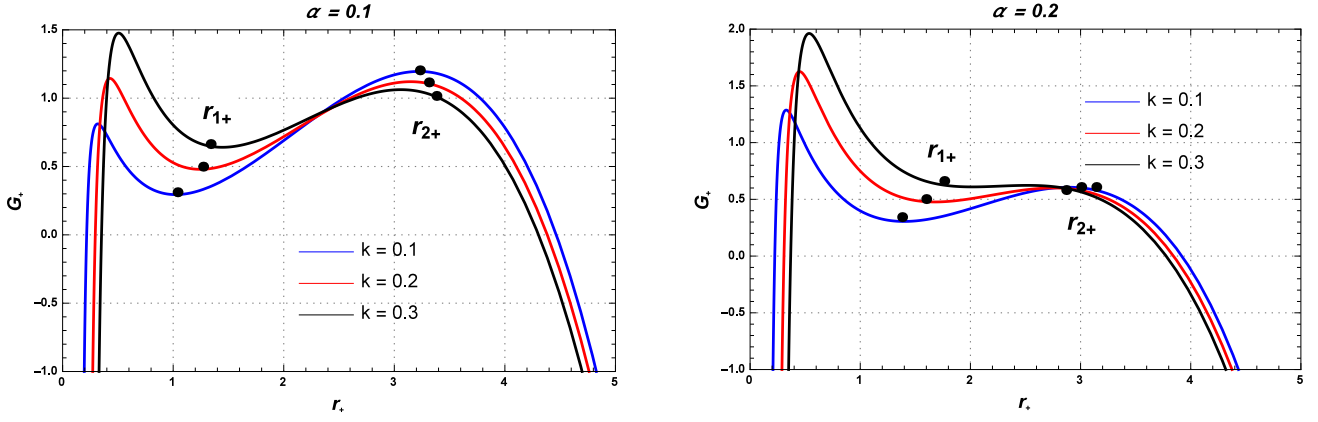
FIG. 4. The Gibbs free energy G_+ versus r_+ with different value of deviation parameter k for $\alpha = 0.1$ and $\alpha = 0.2$ with fixed value of $M = 1$ and $l = 10$.

α. For $r > r_{1+}$, the free energy is an increasing function of r_+ and remains positive and attains the local maximum value at r_{2+}. After $r = r_{2+}$, the slope of Gibbs free energy turns negative and, therefore, the theory provides the natural Hawking-Page phase transition. The various numerical values are tabulated in the TABLE II. Here, we can also see that the Gibbs free energy (G_+) has a minimum and a maximum locally regarding the extremal points of the temperature where the heat capacity diverges.

	$\alpha = 0.1$					$\alpha = 0.2$			
r_{1+}	r_{2+}	T_+	C_+	G_+	r_{1+}	r_{2+}	T_+	C_+	G_+
1.012	3.218	Maximum	Diverge	Loc. Max.	1.405	2.881	Minimum	Diverge	Loc. Min.
1.251	3.148	Maximum	Diverge	Loc. Max.	1.714	2.754	Minimum	Diverge	Loc. Min.
1.447	3.063	Maximum	Diverge	Loc. Max.	2.09	2.515	Minimum	Diverge	Loc. Min.

TABLE II. The numerical values of the local maxima and minima to characterize the nature of T_+, C_+, and G_+.

IV.   VAN DER WAALS FLUID

The aim of this section is to consider the resulting black hole as a Van der Waals fluid and calculate the $P - v$ criticality. As we know, the negative cosmological constant induces a thermodynamic pressure (i.e. $\Lambda = -8\pi P_+$ with $G = \hbar = c = 1$) in the extended thermodynamics. The thermodynamic volume V plays the role of conjugate to pressure and can be interpreted as the change in the mass under the variations in the Λ having fixed horizon area. The mass M is then understood as an enthalpy.

The temperature T_+ in tandem to the above identifications of thermodynamic pressure and conjugate volume lead the following equation of state: Using the and volume V, we obtain the following equations of state:

$$P_+ = \frac{1}{4\pi r^4 (2r_+^2 - k)} \left[6\pi r_+^3 T (r_+^2 + 4\alpha) + 3(kr_+^2 - r_+^4 + 2k\alpha) \right], \quad v = 2r_+, \tag{26}$$

where the v is a specific volume.

The critical points appear at isotherms T_c where pressure has an inflection point at P_c and v_c satisfying conditions [10,14]

$$\left(\frac{\partial P_+}{\partial r_+} \right)_{T_+} = 0, \qquad \left(\frac{\partial^2 P_+}{\partial r_+^2} \right)_{T_+} = 0. \tag{27}$$

The critical radius can be calculated numerically from the relation

$$\frac{2r^8 - 24r^6\alpha - k^2(3r^4 + 16r^2\alpha - 48\alpha^2) - 12k(r^6 + 9r^4\alpha + 36r^2\alpha^2)}{4\pi r^6 (kr^2 + 2r^4 - 4k\alpha + 24r^2\alpha)(k - 2r^2)} = 0. \tag{28}$$
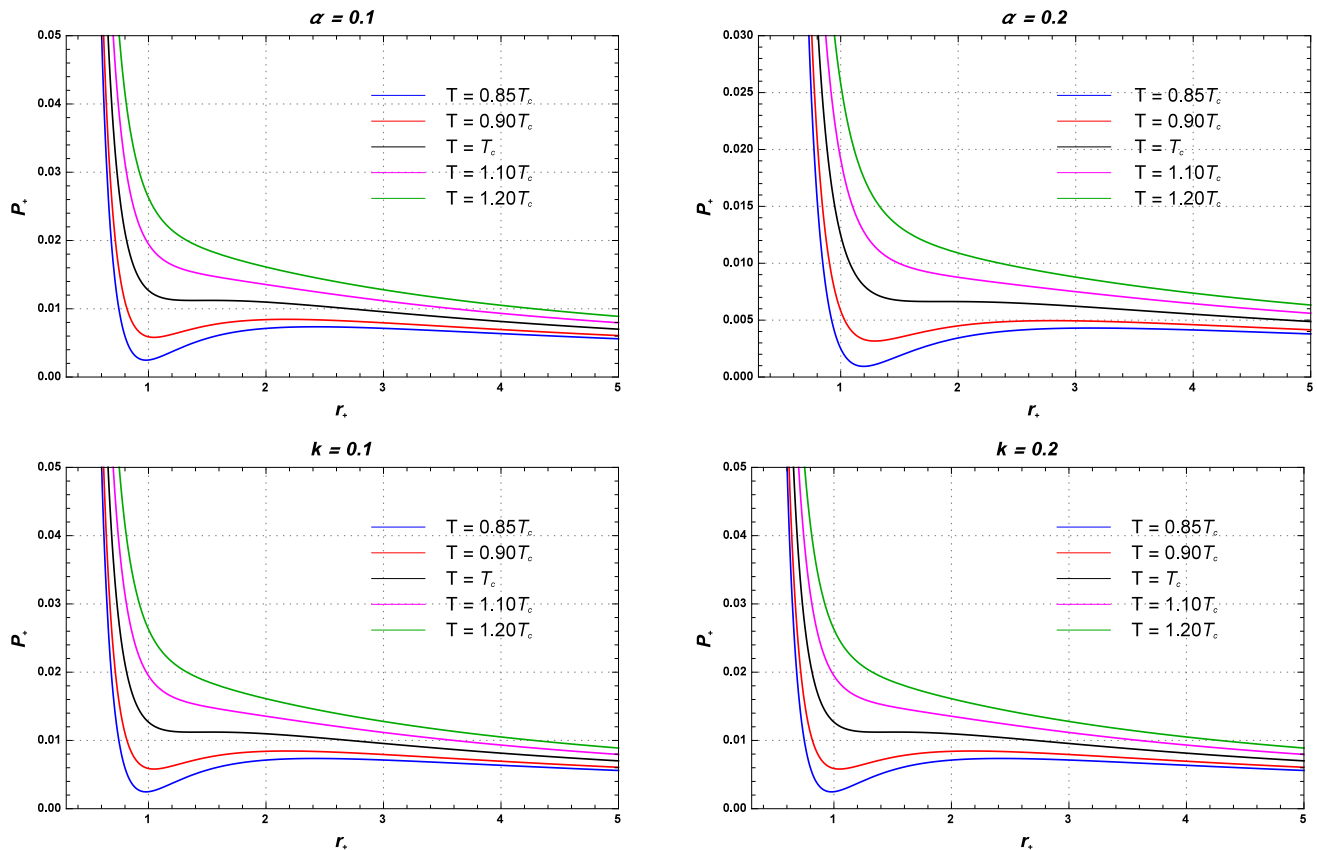
FIG. 5. P_+ versus r_+ with different value of deviation parameter k for $\alpha = 0.1$ and $\alpha = 0.2$ at critical temperature T_c.

The fluid behavior of the regular *AdS* EGB black holes can be seen from the $P_+ - r_+$ diagram in FIG. 5.

The Eq. (28) can not be solved analytically and, therefore, the critical radius r_c, critical pressure P_c and the critical temperature T_c are obtained numerically. The numerical values are presented in TABLES III and IV for different values of α and k. It can be seen that the critical radius r_c increases with the increase in the parameters k and α,

k	r_c	T_c	P_c	$P_c\,r_c/T_c$
0.1	1.453	0.123	0.0225	0.2173
0.2	1.689	0.110	0.0176	0.2425
0.3	1.884	0.100	0.0146	0.2518
0.4	2.055	0.093	0.0125	0.2558
0.5	2.209	0.087	0.0107	0.2579

TABLE III. The critical temperature T_c, critical pressure P_c and $P_c\,r_c/T_c$ corresponding different value of $k = 0.1$ with fixed value of $\alpha = 0.1$.

however, the critical pressure P_c and temperature T_c decrease with increase in k and α. Incidentally, the universal ratio $P_c r_c/T_c$ increases with the parameters k and α. It is worth mentioning that the critical radius increases with decrease in the critical pressure and critical temperature.

V.   QNMS IN EKILON LIMIT

QNMs are usually predicts the stability of the given black holes perturbed by an external field or black hole geometry. QNMs also provide the information regarding gravitational waves. In QNM can be discussed by studying the motion of photon in the vicinity of the black hole solution (11). The photon motion limited to equatorial plane

α	r_c	T_c	P_c	$P_c\, r_c/T_c$
0.1	1.453	0.123	0.0225	0.2173
0.2	1.8434	0.0936	0.0138	0.2617
0.3	2.154	0.0785	0.0094	0.3216
0.4	2.423	0.0690	0.0073	0.4069
0.5	2.662	0.0623	0.0060	0.5381

TABLE IV. The critical temperature T_c, critical pressure P_c and $P_c\, r_c/T_c$ corresponding to the different value of $\alpha = 0.1$ with fixed value of $k = 0.1$.

$(\theta = \pi/2)$ is described by the following Lagrangian:

$$\mathcal{L} = -g_{tt}\dot{t}^2 + g_{rr}\dot{r}^2 + g_{\theta\theta}\dot{\theta}^2 + g_{\phi\phi}\dot{\phi}^2 + g_{\psi\psi}\dot{\psi}^2, \tag{29}$$

where dot denotes the derivative with respect to affine parameter. The corresponding Hamiltonian is given by

$$\mathcal{H} = \frac{1}{2}g^{ij}p_i p_j = 0, \tag{30}$$

and the generalized momenta are given by

$$p_t = \frac{\partial \mathcal{H}}{\partial \dot{t}} = \text{constant} \equiv E, \qquad p_r = \frac{\partial \mathcal{H}}{\partial \dot{r}} = g_{rr}\dot{r}, \qquad p_\theta = \frac{\partial \mathcal{H}}{\partial \dot{\theta}} = g_{\theta\theta}\dot{\theta},$$

$$p_\phi = \frac{\partial \mathcal{H}}{\partial \dot{\phi}} = \text{constant} \equiv -L, \qquad p_\psi = \frac{\partial \mathcal{H}}{\partial \dot{\psi}} = g_{\psi\psi}\dot{\psi}. \tag{31}$$

Here, E and L refer to the energy and the angular momentum per unit rest mass of the test particle, respectively. The equations of motion associated with the photon in the Hamiltonian formalism are given by

$$\dot{t} = \frac{\partial \mathcal{H}}{\partial p_t} = -\frac{p_t}{g_{tt}}, \quad \dot{r} = \frac{\partial \mathcal{H}}{\partial p_r} = -\frac{p_r}{g_{rr}}, \quad \dot{\theta} = \frac{\partial \mathcal{H}}{\partial p_\theta} = \frac{p_\theta}{g_{\theta\theta}},$$

$$\dot{\phi} = \frac{\partial \mathcal{H}}{\partial p_\phi} = \frac{p_\phi}{g_{\phi\phi}}, \quad \dot{\psi} = \frac{\partial \mathcal{H}}{\partial p_\psi} = \frac{p_\theta}{g_{\psi\psi}}. \tag{32}$$

since the above Hamiltonian does not depend on the coordinates t, ϕ and ψ. So, the null geodesics equation is written by

$$\dot{r}^2 + V_{eff}(r) = 0, \qquad \text{with} \qquad V_{eff} = f(r)\left(\frac{L^2}{r^2} - \frac{E^2}{f(r)}\right). \tag{33}$$

For a circular null geodesics, the effective potential must necessarily hold the following conditions:

$$V_{eff} = 0, \qquad \text{and} \qquad \frac{\partial V_{eff}}{\partial r} = 0. \tag{34}$$

These conditions describe the radius of the photon sphere. These conditions lead to the equation of the photon radius as

$$kM - 2Mr^2 + e^{k/r^2}r^2\sqrt{1 + \frac{8M\alpha e^{k/r^2}}{r^4} + \frac{8\Lambda\alpha}{3r^2}} = 0. \tag{35}$$

This equation can not be solved analytically, so we can calculate the photon radius r_p, numerically. The numerical values are presented in TABLE V. From this TABLE, we can see that the photon radius increases along with increasing deviation parameter and GB coupling.

The QNMs frequency ω in the eikonal limit can be estimated by the virtue of the photon sphere as follows

$$\omega = l\Omega - i\left(n + \frac{1}{2}\right)|\Lambda|, \tag{36}$$

α	r_p			
	$k = 0.1$	$k = 0.2$	$k = 0.3$	$k = 0.4$
0.1	1.4381	1.4574	1.4726	1.4840
0.2	1.4503	1.4783	1.5021	1.5169
0.3	1.4728	1.5154	1.5479	1.5727
0.4	1.5298	1.6023	1.6817	1.6954

TABLE V. The numerical values of photon radius corresponding to the GB coupling parameter and devation parameter with $M = 1$, where $l = 1$ and $n = 0$.

k	r_p			
	$\alpha = 0.1$	$\alpha = 0.2$	$\alpha = 0.3$	$\alpha = 0.4$
0.1	1.438	1.450	1.472	1.529
0.2	1.457	1.478	1.515	1.603
0.3	1.472	1.500	1.547	1.654
0.4	1.484	1.516	1.572	1.695
0.5	1.491	1.528	1.591	1.727

TABLE VI. Values of photon radius corresponding to the GB coupling parameter (α) and devation parameter (k) with $M = 1$, where $l = 1$ and $n = 0$.

where n is the overtone number and l is the angular quantum number of perturbation. However, Ω is the angular velocity and Λ is the Lyapunov exponent of the photon sphere with following expressions:

$$\Omega = \frac{\sqrt{f(r_p)}}{r_p} \qquad \text{and} \qquad \Lambda = \frac{\sqrt{f(r_p)(2fr_p - r_p^2 f''(r_p))}}{\sqrt{2}r_p}. \tag{37}$$

Here r_p denotes radius of photon sphere (called as photon radius).

The real and imaginary parts of the QNMs of black hole solution (11) for different values of deviation parameter and GB parameter are depicted in the FIG. 6 and FIG. 7. These diagrams help us to investigate the effects of the
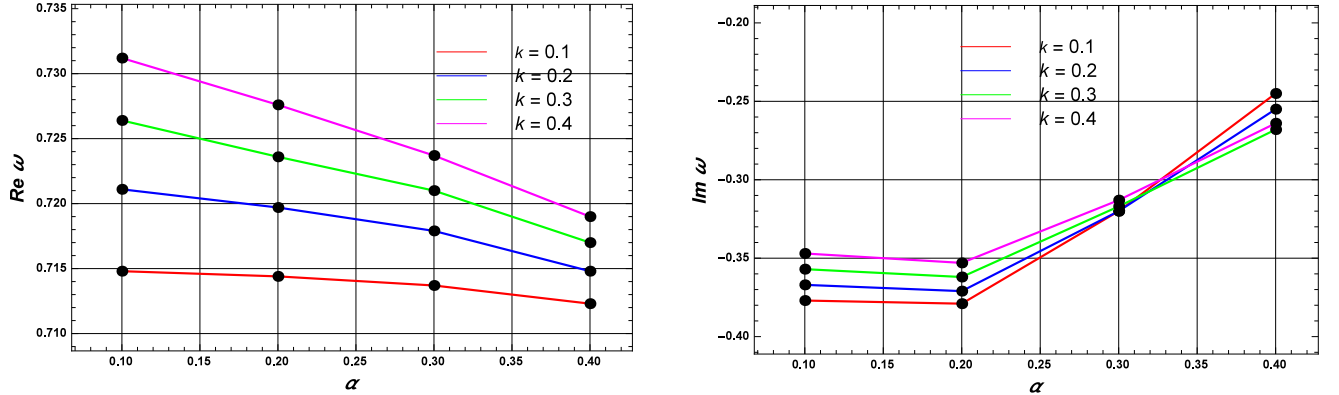

FIG. 6. The plot of real part (left panel) and imaginary part (right panel) of QNMs versus GB parameter with different k with fixed M and l.

black hole parameters on the QNMs. Here, we see that the real part of the QNMs is a decreasing function of the GB parameter. However, real part of the QNMs increases with deviation parameter. On the other hand, the imaginary part of the QNMs with respect to the GB parameter first decreases very slowly (almost constant) and then increases sharply. Also, the imaginary part of the QNMs increases with deviation parameter (more significantly for large α).

The signature of the imaginary part of the QNMs characterizes the stability of black hole. Im $\omega < 0$ corresponds to stable modes of black hole and Im $\omega > 0$ corresponds to unstable modes. The imaginary part of the QNMs for the obtained black hole solution (11) is negative (See Fig. 6 and 7). This confirms that the modes of the obtained black hole solution (11) are stable.
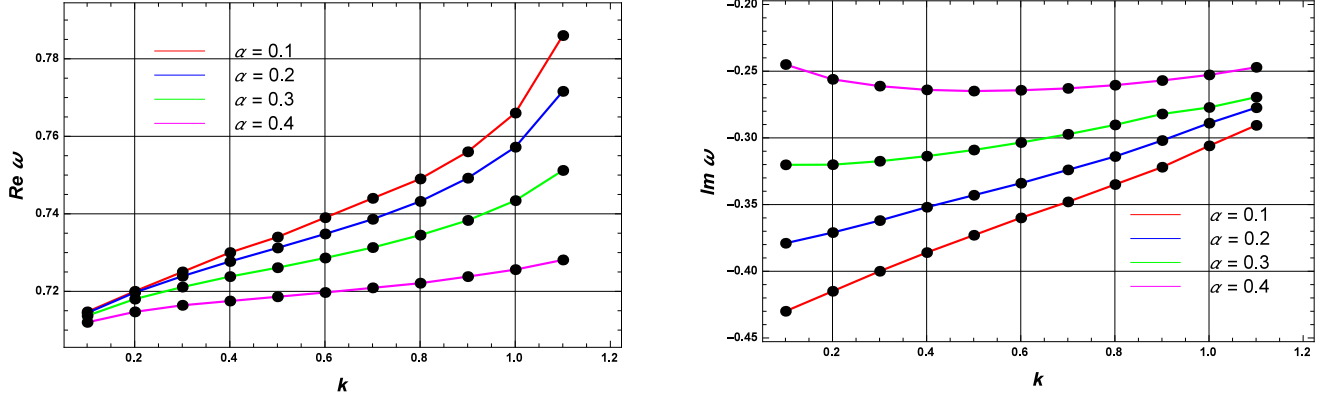
FIG. 7. The plot of real part (left panel) and imaginary part (right panel) of QNMs versus deviation parameter with different k with fixed M and l.

We list the numerical values of QNMs frequency corresponding various values of parameters in TABLES VII and VIII.

α	$k = 1$ ω=Re ω − Im ω	$k = 2$ ω=Re ω − Im ω	$k = 3$ ω =Re ω − Im ω	$k = 4$ ω=Re ω − Im ω
0.1	0.71489 - 0.37765 i	0.721135 - 0.36758 i	0.726456 - 0.35734 i	0.73125 - 0.34703 i
0.2	0.71440 - 0.37984 i	0.719702 - 0.37125 i	0.723687 - 0.36266 i	0.72764 - 0.35300 i
0.3	0.71376 - 0.32043 i	0.717979 - 0.32024 i	0.721104 - 0.31778 i	0.72375 - 0.31388 i
0.4	0.71238 - 0.24545 i	0.714816 - 0.25595 i	0.714815 - 0.26844 i	0.71756 - 0.26416 i

TABLE VII. The numerical values of QNMs corresponding to the GB coupling parameter (α) and devation parameter (k) with $M = 1$, where $l = 1$ and $n = 0$.

k	$\alpha = 0.1$ ω=Re ω − Im ω	$\alpha = 0.2$ ω=Re ω − Im ω	$\alpha = 0.3$ ω=Re ω − Im ω	$\alpha = 0.4$ ω=Re ω − Im ω
0.1	0.7147 -0.4307 i	0.7144 -0.3797 i	0.7137 -0.3202 i	0.71241 -0.245 i
0.2	0.7208 -0.4151 i	0.7197 -0.3712 i	0.7180 -0.3201 i	0.7147 -0.2561 i
0.3	0.7258 -0.4004 i	0.7239 -0.3621 i	0.7211 -0.3175 i	0.7164 -0.2612 i
0.4	0.7303 -0.3866 i	0.7277 -0.3528 i	0.7238 -0.3137 i	0.7175 -0.2640 i
0.5	0.7347 -0.3733 i	0.7312 -0.3435 i	0.7261 -0.3091 i	0.7186 -0.2649 i
0.6	0.7391 -0.3607 i	0.7348 -0.3341 i	0.7286 -0.3035 i	0.7197 -0.2643 i
0.7	0.7440 -0.3482 i	0.7386 -0.3245 i	0.7313 -0.2973 i	0.7209 -0.2629 i
0.8	0.7496 -0.3356 i	0.7432 -0.3143 i	0.7345 -0.2903 i	0.7221 -0.2605 i
0.9	0.7568 -0.3220 i	0.7492 -0.3028 i	0.7383 -0.2821 i	0.7238 -0.2570 i
1.0	0.7669 -0.3061 i	0.7572 -0.2891 i	0.7434 -0.2772 i	0.7256 -0.2528 i
1.1	0.7861 -0.2806 i	0.7716 -0.2674 i	0.7512 -0.2695 i	0.7281 -0.2471 i

TABLE VIII. The numerical values of QNMs corresponding to the GB coupling parameter (α) and devation parameter (k) with $M = 1$, where $l = 1$ and $n = 0$.

VI.   RESULTS AND CONCLUSION

In this work, we have considered a EGB gravity coupled to the NLED in $5D$ AdS spacetime and constructed a new regular black hole solution in AdS spacetime. The obtained solution is a generalized version of $5D$ Schwarzschild-Tangherlini black hole, $5D$ AdS regular Schwarzschild black hole and Boulware-Deser black hole. We have found that the black hole solution exhibits two horizons, namely, the Cauchy and event horizon. There exist different critical

horizons corresponding to different GB parameter that characterize the extremal/non-extremal nature of black holes. The size of the black holes decrease with the increasing GB parameter.

Furthermore, we have studied the thermodynamics of the resulting solution by deriving horizon mass, Hawking temperature and entropy of the black hole. We have found that the black hole satisfies the modified first law of thermodynamics. The stabilities of black hole are discussed by estimating both the heat capacity and Gibbs free energy. The diagrams confirmed that there exist double phase transitions, one from small stable black hole to large unstable black hole and other from smaller unstable black hole to larger stable black hole. The Gibbs free energy analysis confirms the existence of (local) minimum and maximum associated to the extremal points of the Hawking temperature. The fluid nature of black hole is also studied. We have observed that the critical values depend on GB coupling parameter and deviation parameter considerably. For instance, the critical radius is an increasing function of the GB coupling parameter and deviation parameter. In contrast, the critical pressure and critical temperature are decreasing function of the GB coupling parameter and deviation parameter.

It is worth discussing QNMs for the $5D$ AdS regular EGB black hole coupled with NLED as QNMs may provide the information regarding gravitational waves. For this purpose, we studied the motion of photon in the vicinity of the black hole solution. The effects of GB coupling and deviation parameters on the real and imaginary parts of the QNMs are also discussed. It will be interesting to establish a the correspondence between the QNMs in the eikonal limit and the shadow radii for such black hole solution of the $5D$ EGB gravity coupled to the NLED in AdS space.

DATA AVAILABILITY STATEMENT AND COMPETING INTERESTS

Data sharing not applicable to this article as no datasets were generated or analysed during the current study. The authors declare no competing interests.

[1] D. Lovelock, J. Math. Phys. **12** (1971) 498.
[2] D. Lovelock, J. Math. Phys. **13** (1972) 874.
[3] N. Deruelle and L. Farina-Busto, Phys. Rev. D **41** (1990) 3696.
[4] S. Nojiri, S. D. Odintsov and M. Sasaki, Phys. Rev. D **71** (2005) 123509.
[5] S. Nojiri and S. D. Odintsov, Phys. Rept. **505** (2011) 59.
[6] K. Aolki, M.A. Gorji, S. Mukohyama, Phys. Lett. B **810** (2020) 135843.
[7] K. Aolki, M.A. Gorji, S. Mukohyama, J. Cosmol. Astropart. Phys. **09** (2020) 014.
[8] D. V. Singh, S. Upadhyay and Md S. Ali, Int. J. Mod. Phys. A **37** (2022) 2250049.
[9] J. M. Bardeen, in Proceedings of GR5 (Tbilisi, URSS, 1968).
[10] T. Tangphati, A. Pradhan, A. Banerjee and G. Panotopoulos, Phys. Dark Univ. **33** (2021) 100877.
[11] J. M. Z. Pretel, A. Banerjee and A. Pradhan, Eur. Phys. J. C **82** (2022) 180.
[12] T. Tangphati, A. Pradhan, A. Errehymy and A. Banerjee, Phys. Lett. B **819** (2021) 136423.
[13] R. P. Singh, B. K. Singh, B. R. K. Gupta and S. Sachan, Can. J. Phys. **100**, 39 (2022).
[14] S. G. Ghosh, D. V. Singh, Rahul Kumar and S. D. Maharaj, Annals of Physics **424** (2021) 168347.
[15] D. V. Singh and S. Siwach, Phys. Lett. B. **408** 135658 (2020).
[16] S. G. Ghosh, Eur. Phys. J. C **75**, 532 (2015).
[17] S. G. Ghosh and S. D. Maharaj, Eur. Phys. J. C **75**, 7 (2015).
[18] D. V. Singh, B. K. Singh and S. Upadhyay, Annals of Physics **434** (2021) 168642.
[19] D. V. Singh, V. K. Bhardwaj and S. Upadhyay, Eur. Phys. J. Plus **137** (2022) 969.
[20] S. Upadhyay and D. V. Singh, Eur. Phys. J. Plus **137** (2022) 383.
[21] M. Cvetic, S. Nojiri and S. D. Odintsov, Nucl. Phys. B **628** (2002) 295.
[22] S. Nojiri, S. D. Odintsov and S. Ogushi, Phys. Rev. D **65** (2002) 023521.
[23] S. Nojiri and S. D. Odintsov, Phys. Rev. D **66** (2002) 044012.
[24] M. Born and L. Infeld, Proc. Roy. Soc. Lond. A **144**, 425 (1934).
[25] D. L. Wiltshire, Phys. Rev. D38, 2445 (1988).
[26] T. Tamaki and T. Torii, Phys. Rev. D62, 061501 (2000).

[27] N. Breton, Phys. Rev. D 67, 124004 (2003).

[28] S. Fernando and D. Krug, Gen. Rel. Grav. 35, 129 (2003).

[29] R. G. Cai, D. W. Pang and A. Wang, Phys. Rev. D70, 124034 (2004).

[30] C. S. Camara, M. R. de Garcia Maia, J. C. Carvalho and J. A. S. Lima, Phys. Rev. D **69**, 123504 (2004).

[31] E. Elizalde, J. E. Lidsey, S. Nojiri and S. D. Odintsov, Phys. Lett. B **574**, 1 (2003).

[32] M. Novello, E. Goulart, J. M. Salim and S. E. Perez Bergliaffa, Class. Quant. Grav. **24**, 3021 (2007).

[33] D. N. Vollick, Phys. Rev. D **78**, 063524 (2008).

[34] W. Javed, R. Babar and A. Ovgun, Phys. Rev. D **100** (2019) 104032.

[35] K. Jusufi, A. Ovgun, A. Banerjee and I. Sakallı, Eur. Phys. J. Plus **134** (2019) 428.

[36] S. G. Ghosh, D. V. Singh and S. D. Maharaj, Phys. Rev. D **97**, 104050 (2018).

[37] D. V. Singh, S. G. Ghosh and S. D. Maharaj, Nucl. Phys. B **981** (2022), 115854.

[38] S. G. Ghosh, A. Kumar and D. V. Singh, Phys. Dark Univ. **30** (2020), 100660.

[39] D. V. Singh, S. G. Ghosh and S. D. Maharaj, Annals Phys. **412** (2020), 168025

[40] A. Kumar, D. Veer Singh and S. G. Ghosh, Eur. Phys. J. C **79** (2019) 275.

[41] J. M. Maldacena, Adv. Theor. Math. Phys. **2** (1998) 231.

[42] S. S. Gubser, I. R. Klebanov and A. M. Polyakov, Phys. Lett. B **428**, 105 (1998).

[43] E. Witten, Adv. Theor. Math. Phys. **2**, 253 (1998).

[44] S. Nojiri and S. D. Odintsov, Phys. Lett. B **471** (1999) 155.

[45] S. Nojiri and S. D. Odintsov, Phys. Lett. B **521** (2001) 87 [erratum: Phys. Lett. B **542** (2002) 301].

[46] E. Witten, Adv. Theor. Math. Phys. **2**, 505 (1998).

[47] J. D. Bekenstein, Lett. Nuovo Cim. **4**, 737 (1972).

[48] J. D. Bekenstein, Phys. Rev. D **7**, 2333 (1973).

[49] S. W. Hawking, Phys. Rev. D **13**, 191 (1976).

[50] A. Strominger and C. Vafa, Phys. Lett. B **379**, 99 (1996).

[51] A. Ashtekar, J. Baez, A. Corichi and K. Krasnov, Phys. Rev. Lett. **80**, 904 (1998).

[52] S. Carlip, Phys. Rev. Lett. **82**, 2828 (1999).

[53] S. N. Solodukhin, Phys. Lett. B **454**, 213 (1999).

[54] S. Upadhyay, Phys. Lett. B **775**, 130 (2017).

[55] S. Upadhyay, B. Pourhassan and H. Farahani, Phys. Rev. D **95**, 106014 (2017).

[56] J. Jing and M. L Yan, Phys. Rev. D **63**, 024003 (2001).

[57] D. Birmingham and S. Sen, Phys. Rev. D **63**, 047501 (2001).

[58] B. Pourhassan, S. Upadhyay, H. Saadat and H. Farahani, Nucl. Phys. B 928, 415 (2018).

[59] S. Upadhyay, Gen. Rel. Grav. **50**, 128 (2018).

[60] S. Nojiri and S. D. Odintsov, Phys. Lett. B **523** (2001) 165.

[61] S. H. Hendi and M. Momennia, J. High Energy Phys. **10** (2019) 207.

[62] R. A. Konoplya, Phys. Rev. D **100**, 044015 (2019).

[63] I. Sachs, J. High Energy Phys. **09** (2008) 073.

[64] C. Liu, T. Zhu, Q.Wu, K. Jusufi, M. Jamil, M. Azreg-Aïnou, and A. Wang, Phys. Rev. D **101**, 084001 (2020).

[65] B. P. Abbott et al. (LIGO Scientific Collaboration and Virgo Collaboration), Phys. Rev. Lett. **116**, 061102 (2016).

[66] Event Horizon Telescope Collaboration, Astrophys. J. Lett. **875**, L4 (2019).

[67] S. Mandal, S. Upadhyay, Y. Myrzakulov and G. Yergaliyeva, arXiv:2207.10085.

[68] S. Hyun and C. H. Nam, Eur. Phys. J. C **79**, 737 (2019).

[69] E. Ayon-Beato and A. Garcia, Gen. Rel. Grav.**37**, 635 (2005).

[70] L. Balart and E. C. Vagenas, Phys. Lett. B **730**, 14 (2014)

[71] L. Balart and E. C. Vagenas, Phys. Rev. D **90**, no. 12, 124045 (2014).

[72] H. Culetu, Int. J. Theor. Phys. **54** (2015) 2855.

[73] D. Wiltshire, Phys. Rev. D **38**, 2445 (1988).

[74] S. Ansoldi, arXiv:0802.0330 [gr-qc].

[75] K.A. Bronnikov, Phys. Rev. D **63**, 044005 (2001).

[76] M. Ma and R. Zhao, Class. Quantum Grav. **31**, 245014 (2014).

[77] R. V. Maluf and J. C. S. Neves, Phys. Rev. D **97**, 104015 (2018).